N90-29005

Kinematics, Controls, and Path Planning Results for a Redundant Manipulator

by Bruce Gretz[1] and Scott Tilley[2]
Ford Aerospace Corporation, Space Systems Division
3825 Fabian Way, Palo Alto, CA 94303

Abstract

The inverse kinematics solution, a modal position control algorithm, and path planning results for a 7 degree of freedom manipulator are presented. The redundant arm consists of two links with "shoulder" and "elbow" joints and a spherical wrist. The inverse kinematics problem for tip position is solved and the redundant joint is identified. It is also shown that a locus of tip positions exists in which there are kinematic limitations on self-motion. A computationally simple modal position control algorithm has been developed which guarantees a nearly constant closed-loop dynamic response throughout the workspace. If all closed-loop poles are assigned to the same location, the algorithm can be implemented with very little computation. To further reduce the required computation, the modal gains are updated only at discrete time intervals. Criteria are developed for the frequency of these updates. For commanding manipulator movements, a 5th-order spline which minimizes jerk provides a smooth tip-space path. Schemes for deriving a corresponding joint-space trajectory are discussed. Modifying the trajectory to avoid joint torque saturation when a tip payload is added is also considered. Simulation results are presented.

Introduction

Configuring and designing robotic systems for space applications involve many considerations not present in terrestrial systems. Safety and versatility are of prime importance. For example, safety concerns create a need for obstacle avoidance algorithms. Versatility demands may necessitate the manipulator's ability to perambulate between locations. Redundant manipulators meet these requirements because the additional degree(s) of freedom allow inclusion of obstacle avoidance algorithms and increase the maneuverability of the manipulator. The redundant joint configuration presently studied consists of two links with identical two degree-of-freedom "shoulder" and "elbow" joints and a spherical wrist, making a total of 7 degrees of freedom. This particular joint geometry has favorable characteristics with respect to singularity avoidance, obstacle avoidance, and simplicity. It is a candidate for use in several NASA applications on the Space Shuttle, Space Station, Polar Platform, and OMV.

Since this paper deals with quantitative results for a representative space-based manipulator, it is necessary to summarize the assumed system requirements. The fundamental task required is a pick-and-place motion involving a payload of mass up to 100 kg and tip forces of 100 N. Speed of operation is not deemed a high priority, so the manipulator has been designed to achieve tip velocities of 0.5 m/sec. The workspace should be roughly 4 m across, therefore the links are each 1.0 m long. As a result, the joint must be capable of exerting 200 Nm of torque to meet the 100 N tip force requirement. Each link has a mass of 30 kg, including the associated joint.

[1]R&D Engineer
[2]Engineering Specialist

Kinematics Analysis

Figure 1 shows the manipulator configuration. The arm consists of two links of length L_1 and L_2 connected by a two degree of freedom rotational joint (the "elbow"). The base link is attached to the ground by an identical joint (the "shoulder"). Each joint has one rotation axis parallel to the inboard link (roll) and one perpendicular to it (pitch). The shoulder roll axis is normal to the ground surface. The joint angles are denoted θ_1, θ_2, θ_3, and θ_4 and called shoulder roll, shoulder pitch, elbow roll, and elbow pitch, respectively. Joint angle limitations are not being considered.

The four degrees of freedom in the shoulder and elbow joints thus provide redundancy for positioning the manipulator tip A three dimensional wrist can then be used to orient the end effector. Assuming a spherical wrist, its kinematics are decoupled from those of the rest of the arm and are not treated in this analysis.

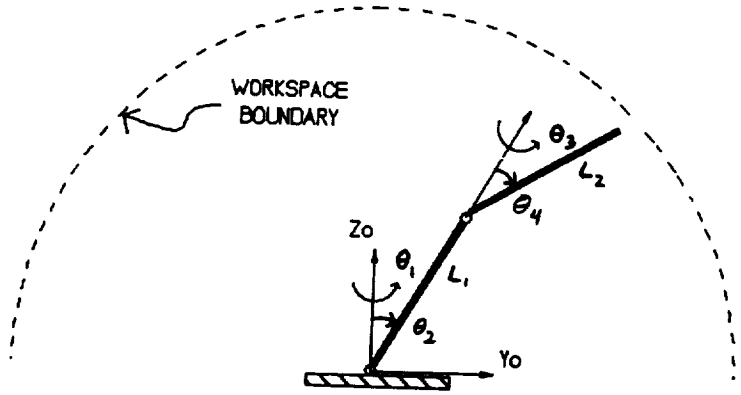

Figure 1: Joint Configuration of Redundant Manipulator

The forward kinematics of the arm are easily solved using a variety of methods. In the present analysis, homogeneous transformation matrices derived from the Denavit-Hartenberg parameters were multiplied together to produce the vector reaching from the base point to the tip [1]. The result is

$$\begin{aligned} x &= L_1 c_1 s_2 + L_2 (c_1 s_2 c_4 - s_1 s_3 s_4 + c_1 c_2 c_3 s_4) \\ y &= L_1 s_1 s_2 + L_2 (s_1 s_2 c_4 + c_1 s_3 s_4 + s_1 c_2 c_3 s_4) \\ z &= L_1 c_2 + L_2 (c_2 c_4 - s_2 c_3 s_4) . \end{aligned} \tag{1}$$

where c_1 denotes $\cos\theta_1$, etc. The reachable workspace is a sphere of radius $L_1 + L_2$ centered at the base.

Every redundant manipulator is capable of self-motion, that is, the tip can be fixed while the joint angles are varied. For the present manipulator, self-motion consists of "orbiting" the elbow joint in a circle. During orbiting all four joint angles must change. In particular, the elbow roll angle varies from 0° to 360°. It follows that for a given tip position, an inverse kinematics solution can be found for any elbow roll angle. The same cannot be said for the other three degrees of freedom, therefore the elbow roll angle is the redundant joint. (For some tip positions, there exists a kinematic limitation on the elbow roll angle. This will be addressed later.)

Specifying the tip position and elbow roll angle does not uniquely determine the other joint angles – there are still four possible solutions. These solutions determine one of two possible positions of the elbow joint and one of two possible orientations of link 1. For example, if the tip lies in the xy-plane (see Figure 1) then a point on the side of link 1 could "face" the z-axis or the xy-plane. Also, the elbow joint may be above or below the xy-plane.

Figure 2 shows an inverse kinematics "tree" containing the equations for these four solutions. The first step in obtaining a solution is arbitrarily choosing the elbow roll angle, θ_3. The elbow pitch angle , θ_4, is found next by examining the triangle whose sides are the two links and the vector from base to tip, $\vec{r}$. Since all three sides are known, the angle between the links is easily computed. Its supplement is θ_4. This solution has two values corresponding to the ambiguity in the sign of the inverse cosine. Physically, this corresponds to the elbow bending "up" or "down" and determines one of the two possible elbow joint positions. Once one of these two configurations is chosen, the appropriate branch of the tree is selected. The shoulder pitch angle, θ_2, is computed next. Its equation is found by manipulation of the forward kinematics equations. The sign ambiguity in this equation corresponds to link 1 facing "up" or "down". This choice of sign determines the final branch of the tree. The shoulder roll angle is now uniquely determined.

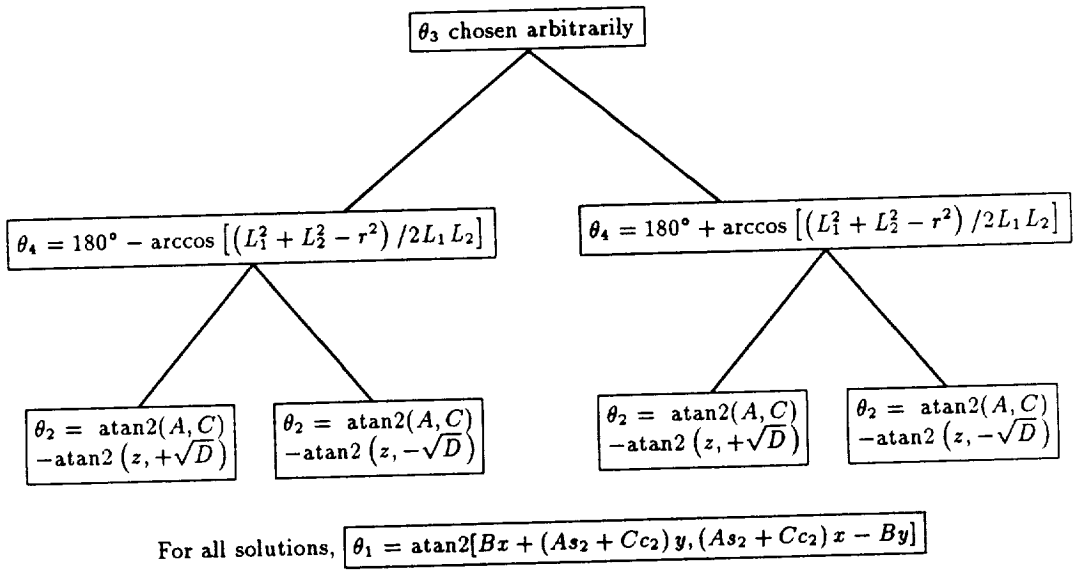

For all solutions, $\theta_1 = \text{atan2}[Bx + (As_2 + Cc_2)y, (As_2 + Cc_2)x - By]$

$$A \equiv L_1 + L_2c_4 \qquad C \equiv L_2s_4c_3$$
$$B \equiv -L_2s_4s_3 \qquad D \equiv A^2 + C^2 - z^2$$

Figure 2: The Four Inverse Kinematics Solutions

It has been noted that for some tip positions, there is a kinematic limitation on self-motion, meaning that the elbow roll angle cannot take on an arbitrary value. Mathematically, this limitation can be derived from the equation for θ_2. If D, equal to $A^2 + C^2 - z^2$, is less than zero, then no solution exists. This occurs when A and C are both "small". A is the length of the arm projected onto the vector parallel to link 1, so A decreases as the arm is folded onto itself. C is proportional to $\cos\theta_3$, thus it decreases as θ_3 nears 90°. From this qualitative analysis two results may be concluded: 1) When the arm is relatively far extended the elbow roll angle can take on any value and thus complete orbiting is possible, and 2) When the arm is folded towards itself the elbow roll angle must be near 0°. Both of these conclusions can be restated rigorously. Assuming $L_1 = L_2 = L$, it can be shown that for tip positions lying outside of the volume defined by two spheres centered at $z = \pm L$ and having radius L, the elbow roll angle may take on any value. For tip positions lying inside of this volume, the elbow roll angle is constrained to

$$|\theta_3| < \arccos\left\{\sqrt{\frac{z^2 - (L_1 - \gamma L_2)^2}{L_2^2(1 - \gamma^2)}}\right\}, \tag{2}$$

where $\gamma \equiv (L_1^2 + L_2^2 - r^2)/(2L_1L_2)$. This range of angles is centered around $\theta_3 = 0$. Figure 3 shows the regions of limited orbit capability.

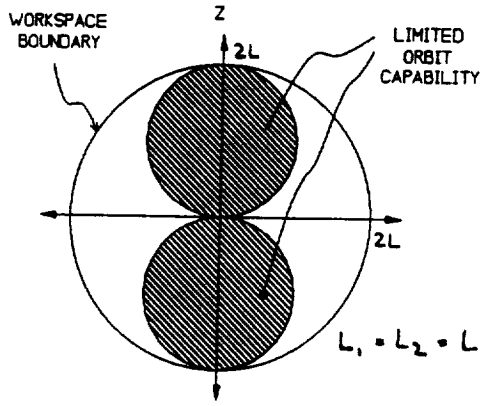

Figure 3: Regions of Limited Orbit Capability

For maximum maneuverability, Figure 3 indicates that it is desirable to keep the workspace near the xy-plane. An interesting parallel exists between this workspace location and the dexterous "workspace" of the human arm. The human arm is kinematically similar to the manipulator if we visualize its "z" axis extending horizontally out the sides of the shoulder. Our arms are most dexterous in front of us, which is near our xy-plane and corresponds to the manipulator area of complete orbit capability.

Controller Design and Analysis

The controller design for a space-based manipulator is primarily driven by requirements to maintain a specified closed-loop bandwidth with a minimum of computational complexity. The bandwidth is specified to accurately follow commanded trajectories. Disturbance rejection and modeling error impacts will be discussed later. Computed torque controllers, which use feedforward, will provide good dynamic response throughout the workspace; however, their computational complexity may preclude their use in space applications. The modal control algorithm presented in this paper is designed to maintain a nearly constant closed-loop dynamic response with a minimum of computation.

The equations of motion of any space manipulator take the form

$$\tau_c = M(\Theta)\ddot{\Theta} + V(\Theta, \dot{\Theta}) + F(\Theta, \dot{\Theta}) - \tau_d, \tag{3}$$

where τ_c is the joint control torque, Θ is a vector of joint angles, M is the mass matrix, and V is the nonlinear "velocity-squared" term of the dynamics, F is the friction terms, and τ_d is the joint disturbance torque arising from tip disturbance torques. For purposes of controller design, V and F can be viewed as a disturbance torques. Therefore, assuming the controller will have sufficient disturbance rejection and/or V and F are sufficiently small, the controller can be designed based on the approximate equations of motion given by

$$\tau_c = M(\Theta)\ddot{\Theta}. \tag{4}$$

If constant gain colocated joint control is applied to a manipulator the dynamic response varies widely throughout the workspace. Equation 4 shows that for slow motions this variation is primarily caused by the changes in the mass matrix as a function of Θ. (Physically, the apparent inertia at each joint changes with arm geometry.)

The modal control algorithm applies colocated joint torques using feedback gains which vary with configuration in order to ensure a nearly constant closed-loop bandwidth throughout the workspace. The feedback gains are computed from the mass matrix as follows. The mass matrix M is always real positive definite and thus may be transformed such that $S^T M S = D$, where D is diagonal and $S^T S = I$. The simplified equations of motion (equation 4) then become

$$S^T M S \ddot{\eta} = S^T \tau_c, \tag{5}$$

where $\eta \equiv S^T \Theta$. The elements of η are called the modal coordinates. Equation 5 may be rewritten as

$$D\ddot{\eta} = u, \tag{6}$$

where $u \equiv S^T \tau$ is the modal control torque. Placing the poles of this system using modal position and rate feedback is almost trivial because D is diagonal. Its diagonal elements are the modal inertias, denoted λ_i. The modal control torque thus takes the form

$$u_i = -(K_{p,i}\eta_i + K_{r,i}\dot{\eta}_i), \tag{7}$$

where $K_{p,i} = \lambda_i \omega_i^2$ and $K_{r,i} = 2\lambda_i \zeta_i \omega_i$ are the ith modal position and rate gains, respectively, which give the closed-loop poles associated with η_i a damping of ζ_i and a frequency of ω_i. The modal control torque is transformed back into joint space to give the joint control torque as

$$\tau_c = -Su = -S\begin{bmatrix} K_p & K_r \end{bmatrix}\begin{Bmatrix} \eta \\ \dot{\eta} \end{Bmatrix} = -S\begin{bmatrix} K_p & K_r \end{bmatrix}\begin{bmatrix} S^T & 0 \\ 0 & S^T \end{bmatrix}\begin{Bmatrix} \Theta \\ \dot{\Theta} \end{Bmatrix}, \tag{8}$$

where K_p and K_r are diagonal matrices containing the position and rate gains given in equation 7. The control torque may be rewritten as

$$\tau_c = -\begin{bmatrix} SK_pS^T & SK_rS^T \end{bmatrix}\begin{Bmatrix} \Theta \\ \dot{\Theta} \end{Bmatrix}. \tag{9}$$

Since eigenvalues are preserved under a similarity transformation, the feedback scheme of equation 9 results in the same closed-loop poles that were assigned to the modal coordinates using equation 7. As a result, a constant dynamic response throughout the workspace is assured for sufficiently slow manipulator motions.

The choice of closed-loop frequency and damping is the result of hard requirements and engineering judgments. The requirements arise from desired tracking accuracy. This will be discussed later. The engineering judgements include considerations of disturbance rejection, positioning accuracy, tip force application, and noise sensitivity. Other factors which impact system stability and performance include structural flexibility, modeling errors, and time delays. Further, the control must be implemented on actuator/drive subsystems which contain their own dynamics [2]. The influence on all of these factors on choice of closed-loop pole location are topics of continuing research.

Reducing Control Computation

Implementing the algorithm described above requires diagonalization of the mass matrix and several matrix multiplications involving S. Much of this computation can be avoided by a simple restriction on the pole placement, namely, that each of the poles corresponding to the η_i be placed at the same location. In this case, the position and rate gain matrices become

$$\begin{aligned} K_p &= D\omega^2 \\ K_r &= 2D\zeta\omega, \end{aligned} \tag{10}$$

where ζ and ω are the damping and frequency, respectively, of that one pole location. As a result, equation 9 reduces to

$$\tau_c = -\begin{bmatrix} M\omega^2 & 2M\zeta\omega \end{bmatrix}\begin{Bmatrix} \Theta \\ \dot{\Theta} \end{Bmatrix}. \tag{11}$$

The control gains can thus be computed simply by multiplying the mass matrix by a scalar. The restriction that all modal poles be placed at the same location is not unrealistic. For trajectory following, it is only necessary that their frequencies are sufficiently high and their damping is adequate.

Further computation reduction can be achieved by updating the control gains (the matrix of equation 9) less frequently than every microprocessor cycle. Thus the same control gains are used for several cycles even though the manipulator configuration is changing slightly. The gain computation can then be spread over several cycles with the gains being updated only after the computation is complete.

Analysis has been performed to determine how often these updates need to take place. The minimum gain update frequency depends on how fast the mass matrix is changing since the gains are computed from it. For the present manipulator, the mass matrix is most sensitive to the shoulder and elbow pitch angles. The shoulder pitch angle changes the apparent inertia about the shoulder roll joint because it moves the entire manipulator either closer or farther from that joint's axis. The elbow pitch angle folds the arm either in or out and thus changes the apparent inertia about both shoulder joints. As a result, the gain update frequency should be set according to expected pitch angle rates for a given manipulator motion. It has been found from simulation that the gains should be updated no less than once every 5° of either pitch angle rotation. Such rotations change the terms in the inertia matrix by less than 10%, provided the arm is not fully extended.

Tip-Space Stiffness and Contact Forces

Of interest in the design of a position controller are the forces of contact generated when the manipulator tip approaches a desired location and touches the environment. These forces are important in determining how well a manipulator performs a given task and whether there is a possibility of damaging the environment. For these reasons, it is important to quantify the contact forces which a given controller generates.

Contact forces are generated by a manipulator under position control when an obstacle prevents the tip from reaching its commanded position. For example, if the tip is commanded to a position behind a wall (due to position sensor inaccuracies or an error in modeling the environment) the tip will be stopped by the wall but continue to exert a force on it as the tip tries to reach the commanded position. The magnitude of the resulting contact force depends on how far the commanded position is behind the wall and the Cartesian "stiffness" of the control system. This stiffness can be expressed as a matrix K in the relation

$$F = -K\Delta x, \tag{12}$$

where F is the force acting on the wall and Δx the distance from the commanded position to the wall. Equation 12 also expresses the relation between a force exerted on the tip in free space and the resulting tip deflection.

Any manipulator under position control exhibits such a stiffness due to position feedback in the controller. In steady-state, the control law can be written $\tau_c = -G\Delta\Theta$, where G is the position gain matrix given by $G = SK_pS^T$ when using modal control (see equation 9). It is well-known that the Jacobian J relates tip deflections to joint deflections by $J\Delta\Theta = \Delta x$ and tip forces to joint torques by $J^TF = \tau$. Substituting these two relations into the steady-state control law above and rearranging yields

$$F = -(JSK_p^{-1}S^TJ^T)^{-1}\Delta x. \tag{13}$$

Thus the apparent stiffness matrix of the manipulator under modal control is $K = (JSK_p^{-1}S^TJ^T)^{-1}$. The properties of this matrix as a function of the controller gains and joint angles is a topic of continuing research.

Path Planning for a Redundant Manipulator

The simplest problem in path planning is computing a tip-space position, velocity, and acceleration trajectory that moves the end effector from one point to another. A 5th-order spline has been chosen for this purpose because it can give zero velocity and acceleration at the end points. The solution is

$$x(t) = x_i + (6\tau^5 - 15\tau^4 + 10\tau^3)(x_f - x_i), \tag{14}$$

where x_i and x_f are the initial and final positions and τ (defined as t/T) is normalized time with T the total maneuver time [3]. It can be shown that this spline also gives the minimum jerk for any polynomial trajectory. Hollars recommends that the controller have a bandwidth of at least $4/T$ Hz to adequately track this spline. The same spline is used for all three tip-space coordinates. As a result the trajectory is a straight line between the start and end points.

The next task in path planning is generating a joint-space trajectory corresponding to the desired tip-space trajectory. For redundant manipulators, there exists an infinite number of joint trajectories for each tip trajectory. In the present case there is one redundant degree of freedom, therefore one additional constraint must be added in order to produce a solution. This constraint could arise from considerations of singularity avoidance, obstacle avoidance, tip-space stiffness, etc.

The present manipulator has no internal singularities within the region of complete orbit capability. Therefore, an easy singularity avoidance scheme consists of limiting the workspace to this region. A constraint still needs to be chosen to solve the inverse kinematics. The constraint $\theta_3 = 0$ is one simple possibility. This leaves four possible solutions for the other joint angles (see Figure 2). A single one can be selected based on how the links are to be oriented during the motion (elbow "up" or "down", etc.). This choice could be driven by constraints on the position of the elbow itself arising from obstacle avoidance concerns.

Another possible constraint is minimizing joint velocities. This can be accomplished by resolved-rate control in which a desired tip velocity trajectory is transformed into a joint velocity trajectory. The Jacobian pseudo-inverse is used to find the instantaneous minimum joint velocity. The solution is

$$\dot{\Theta}(t) = J^{\dagger}\dot{X}(t), \tag{15}$$

where $\dot{X}(t)$ is the vector of tip-space coordinates and $J^{\dagger}$ is the Jacobian pseudo-inverse given by $J^{\dagger} = J^T(JJ^T)^{-1}$. This solution minimizes the 2-norm of the joint velocity vector at each point in the trajectory. Several modifications to this method have been proposed in the literature [4,5]. They generally attempt to optimize some other performance criterion or potential function.

One argument for using equation 15 is that it helps avoid singularities because joint velocities tend to increase near them. However, this method causes the tip to follow the desired trajectory exactly, therefore if the trajectory passes close to a singularity then the minimum joint velocity solution can be arbitrarily large. Wampler and Leifer [6] have proposed an interesting modification to this method which causes the tip to deviate from the desired trajectory when it approaches a singularity. In this way an upper bound on joint velocities can be maintained.

For the present manipulator, limiting the workspace to the region of complete orbit capability will avoid all internal singularities. If the manipulator is required to move out of this region then $\theta_3 = 0$ is the recommended constraint because it will avoid orbit angle limits. If the tip is always in this region then either $\theta_3 = 0$ or equation 15 gives acceptable results for simple pick-and-place operations. When constraints involving obstacle avoidance, elbow joint position, or tip stiffness arise, the redundancy can be used to address them.

Path Planning in the Presence of a Tip Payload

Since we are designing a manipulator to perform pick-and-place operations, path planning with a tip payload is of concern. Clearly, executing a trajectory with a tip payload will require larger control torques than tracking the same trajectory without a payload. A nominal trajectory duration for movements without a payload should be selected such that the peak joint torque commanded is a certain fraction of the maximum joint torque. This nominal duration should be varied with trajectory distance in order to keep the average tip velocity constant. This will ensure that the velocity-squared terms and the inertia term of the equations of motion maintain the same relative magnitude (see equation 3).

When a payload is added, the nominal trajectory must be modified in order to ensure the same peak joint torque command. Using simple results from the dynamics of accelerating a point mass, we can assume that the maximum control torque required to execute a trajectory is inversely proportional to the square of the maneuver time. That is,

$$\tau_{c,max} \propto \frac{1}{T^2}, \tag{16}$$

where $\tau_{c,max}$ is the maximum control torque and T is the trajectory duration. The first step in modifying the trajectory is running a simulation to determine the peak joint torque commanded when moving the payload through the nominal trajectory duration. Equation 16 can then be used to adjust the maneuver time accordingly. Also, the desired closed-loop pole frequency should be lowered so that it is no higher than that required for tracking. This will minimize the sensitivity of the controller to noise and unmodeled dynamics.

The mass matrix used to compute the control gains should include modeling of the payload. If it does not then the closed-loop poles will have a lower frequency and damping than that desired. As a result, the disturbance and noise rejection may be degraded. Including modeling of the payload in the mass matrix will ensure that the desired closed-loop poles are achieved. Since space-based manipulators will initially be used in highly structured environments, the time of attachment and mass properties of payloads should be readily available.

Simulation Results

This section presents simulations of tip trajectory following with and without a payload using the modal control algorithm and two redundancy management schemes. The starting and ending tip coordinates (in meters) in the x-y-z coordinate system of Figure 1 are $(-0.8, 1.0, 0.6)$ and $(0.6, 1.2, -0.8)$, respectively, giving a trajectory length of about 2 m. Note that the line connecting these points lies completely within the area of complete orbit capability. The control gains are updated every 0.25 sec and the payload is assumed to be a point mass of 100 kg located at the tip.

Figure 4 shows the response with no payload using the $\theta_3 = 0$ constraint. All closed-loop pole frequencies are set to 2.4 rad/sec, which is the minimum required for a 10 sec slew. In the first plot the actual and commanded tip motion are shown. Although the actual tip motion lags slightly behind the desired trajectory, it converges accurately to the desired end position at the end of the maneuver. Note that the discrete gain updating causes jumps in the commanded joint torques. Since joint dynamics are not modeled here, the commanded torque is equal to the applied torque. In actuality, the dynamics of the joint motor will smooth these jumps while not degrading the tracking accuracy. Modeling joint dynamics is currently being researched [2].

Figure 5 shows the same simulation except that the pseudo-inverse is used to generate the joint trajectory. Notice how θ_3 attains a final angle of about 35° in order to decrease the average velocity of the other three joints. Otherwise, the performance is the same as before. Figure 6 shows the simulation of Figure 4 except that a 100 kg payload has been added. Another simulation showed that the maximum control torque with this payload and a maneuver time of 10 sec is about 12 Nm. Therefore, using equation 16 and the fact that the previous simulations have maximum

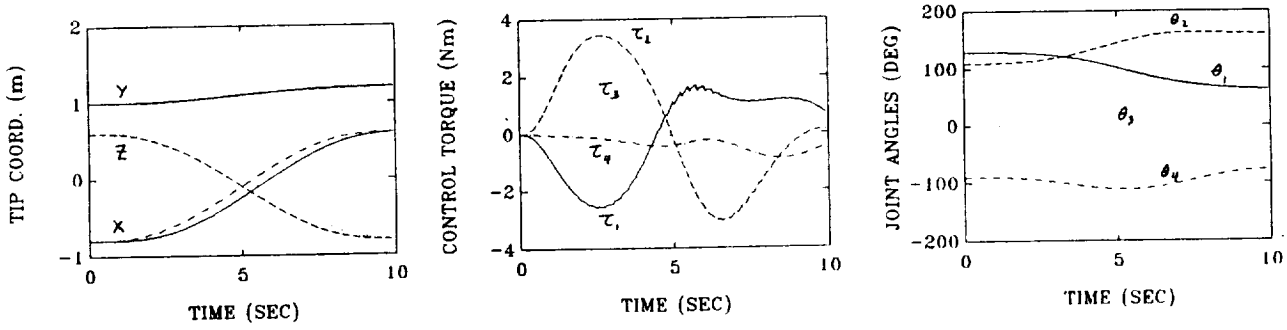

Figure 4: Simulated Maneuver with $\theta_3 = 0$ Constraint

control torques of 3 Nm, the maneuver time was lengthened by a factor of 2 ($= \sqrt{12/3}$) to bring the maximum control torque back to 3 Nm. In addition, the closed-loop poles were reduced to 1.2 rad/sec to match the increase in maneuver time. The tracking performance is as good as that with no payload.

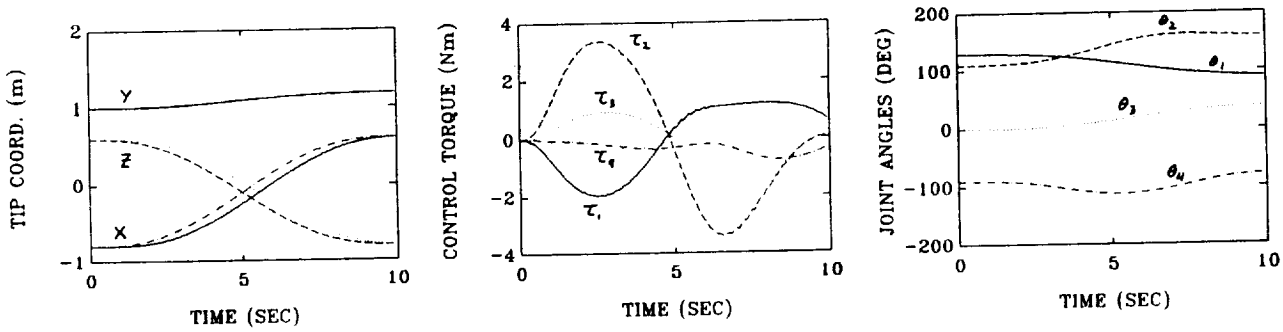

Figure 5: Simulated Maneuver with Minimum Joint Velocity Constraint

Conclusions

The inverse kinematics solution, a modal position control algorithm, and path planning results for a 7 degree of freedom manipulator have been presented. After arbitrarily choosing the elbow roll angle, the redundant degree of freedom, the inverse kinematics has four solutions. Each solution corresponds to a different orientation of the links in space. It is also shown that a locus of tip positions exists in which there are kinematic limitations on the orbit angle.

A computationally simple modal position control algorithm has been developed which guarantees a nearly constant closed-loop dynamic response throughout the workspace. The algorithm consists of diagonalizing the mass matrix into four modal inertias and computing feedback gains to control the modal coordinates. This controller is able to reject the disturbance arising from the unmodeled velocity-squared terms. If all closed-loop poles are assigned to the same location, the algorithm can be implemented with very little computation. To further reduce the required computation, the modal gains are at discrete time intervals. An update frequency of every 5° of either pitch angle

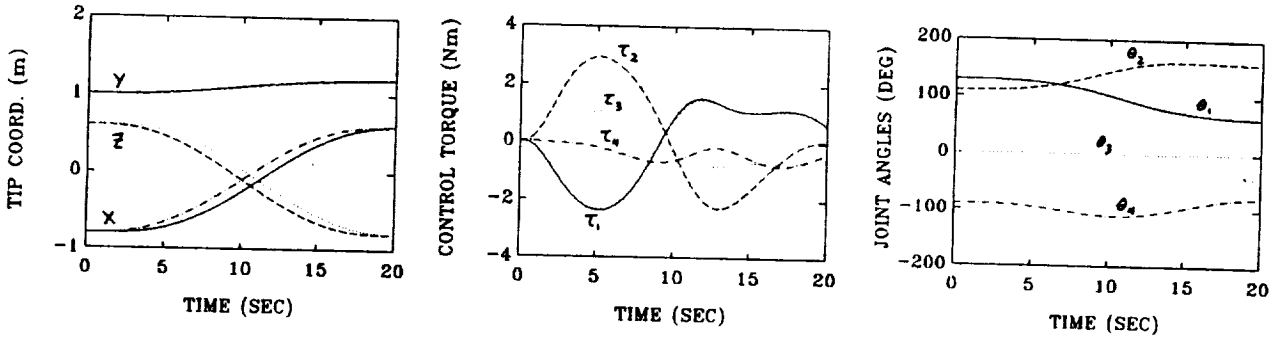

Figure 6: Simulated Maneuver with 100 kg Payload

motion significantly reduces computation without degrading performance.

For commanding manipulator movements, a 5th-order spline with zero velocity and acceleration at the end points provides a smooth tip-space path. The frequencies of the closed-loop poles should be at least $4/T$ Hz, where T is the trajectory duration, to maintain adequate tracking. The best singularity avoidance scheme is keeping the tip trajectory in the region of complete orbit capability. The orbit angle can then be used to address other constraints such as obstacle avoidance or tip-space stiffness. A method is presented for modifying the trajectory duration when a payload is added to maintain a constant joint control torque. The payload should be modeled in the mass matrix to allow accurate control over the closed-loop bandwidth.

References

[1] Craig, J.J., "Introduction to Robotics - Mechanics & Control", Addison-Wesley, 1986.

[2] Tilley, S.W., Emerick, K., Francis, C., and Hollars, M.G., "Preliminary Results on Noncolocated Torque Control of Space Robot Actuators", presented at the NASA Conference on Space Telerobotics, Pasadena, CA, January 1989.

[3] Hollars, M.G., Experiments in End-Point Control of Manipulators with Elastic Drives", Stanford University PhD Thesis, May 1988.

[4] Dubey, R. and Luh, J.Y.S., "Performance Measures and Their Improvement for Redundant Robots", presented at Winter Annual Meeting of ASME, Anaheim, CA, from *Robotics: Theory and Applications*, DSC vol. 4, pp. 143-151, December 1896.

[5] Walker, Ian D. and Marcus, Steven I., "Subtask Performance by Redundancy Resolution for Redundant Robot Manipulators", Communication in *IEEE Journal of Robotics and Automation*, vol. 4, no. 3, pp. 350-354, June 1988.

[6] Wampler II, C.W. and Leifer, L.J., "Applications of Damped Least-Squares Methods to Resolved-Rate and Resolved-Acceleration Control of Manipulators", *Journal of Dynamic Systems, Measurement, and Control*, vol. 110, pp. 31-38, March 1988.